RODIN

-

Suspended Graphene Nanostructures

FINAL REPORT

NMP2009-2.1-1 **Project No: 246026**

11/27/2013

CHALMERS

Aalto University

TU Delft
Technische Universiteit Delft

ICFO
The Institute of Photonic Sciences

ICN
Institut Català de Nanotecnologia

TARTU ÜLIKOOL 1632 UNIVERSITAS TARTUENSIS

UNIVERSITY OF CAMBRIDGE

DIARC

NOKIA

RENESAS
Renesas Mobile

Contents

Executive summary

For graphene to become an integral material component in nanotechnology, developments on several levels in the fabrication process are necessary. To address the relevant challenges at all stages, the RODIN project targeted the fabrication of frequency tuneable, high-quality graphene resonators using suspended graphene. These nano-mechanical resonators hold promise as RF-components which can be used for instance in the front ends of RF-transceivers. There is currently no other technology available that could bring tunability to a high-quality resonator and thus a filter, enabling the adaptivity benefiting current cellular multiradio systems and future cognitive radio architectures.

Manufacturing suspended structures, where graphene does not rest on a substrate, puts an extra high demand on nanoscale manipulation and electrical contacting. Hence, one major objective of the project has been to develop and perfect graphene nanofabrication technology well beyond the current state of the art. An important outcome of the project is the knowledge and technology advancement in the field of nanomanipulation of suspended graphene. To avoid the impact of the substrate on graphene properties, suspended structures may have to be used. This is true also for other devices than nanoresonators. For successful implementation and large scale production of IT-devices or graphene based integrated circuits, the ability to fabricate multiple devices by sculpting a single sheet and applying in-situ post-processing techniques to enhance mobility will be extremely valuable if high yield methods can be realized.

Over the three years of duration, the RODIN project has produced an impressive amount of scientific results advancing graphene production, manipulation and characterization. The results has been disseminated in 55 peer-reviewed publications and presented at more than 75 times at international conferences. The main goal, the demonstration of a frequency tunable nanomechanical resonator was realized towards the end of the project using a design based on wide rectangular few layer graphene sheets. While the demonstrated resonators did not reach the specifications needed for direct implementation as filters in RF-transceiver front ends, their performance did correspond to that from modelling. Based on the verified device models, CAD-models for assessment of resonator based RF-filter design were constructed. The main outcome of the project is that:

Using the resonator design, models, fabrication, characterization and graphene manipulation methods developed in RODIN, graphene mechanical filters in RF-components can be realized. However, in order to reach the target specifications, a state-of-the art industrial fab-facility must be subcontracted for making the chips and methods for better contacting of the graphene to the electrodes should be further developed to enhance performance.

Summary of context and main objectives

While the remarkable electronic structure of graphene has attracted much attention, its mechanical and piezo-resistive properties came into focus comparatively late. This should be contrasted with carbon nanotubes (CNTs): their unique mechanical properties were recognized early on and are already exploited in consumer products (e.g. Li batteries). Indeed, the exceptional strength of CNTs, which stems from the inherent strength of the sp^2 carbon bond, is present also in graphene. For CNTs the chirality dictates the electronic properties, which has meant that no advanced CNT-based electronic devices are on the market today due to difficulties with chirality controlled production. In the same way, many of the early proposed graphene devices depended sensitively on the detailed atomic arrangement or functionalization at the edges. Hence, learning from the experience with CNTs, before other electronic graphene devices are fully developed, it will most likely be graphene-based mechanical devices, electrical interconnects/electrodes, or graphene composites and thin films that will first enter the consumer market. With such more robust nanotechnology applications in mind the RODIN project aimed at studying the mechanical, electromechanical and electrical properties of graphene-based nanomaterials (from single- up to few-layer graphene structures as well as sp^2-rich graphitic carbon thin films).

For graphene to become an integral material component in nanotechnology, developments on several levels in the fabrication process are necessary. To address the relevant challenges at all stages, the RODIN project targeted the fabrication of frequency tuneable, high-quality graphene resonators using suspended graphene. Manufacturing suspended structures, where graphene does not rest on a substrate, puts an extra high demand on nanoscale manipulation and electrical contacting. Hence, one major objective of the project has been to develop and perfect graphene nanofabrication technology well beyond the current state of the art.

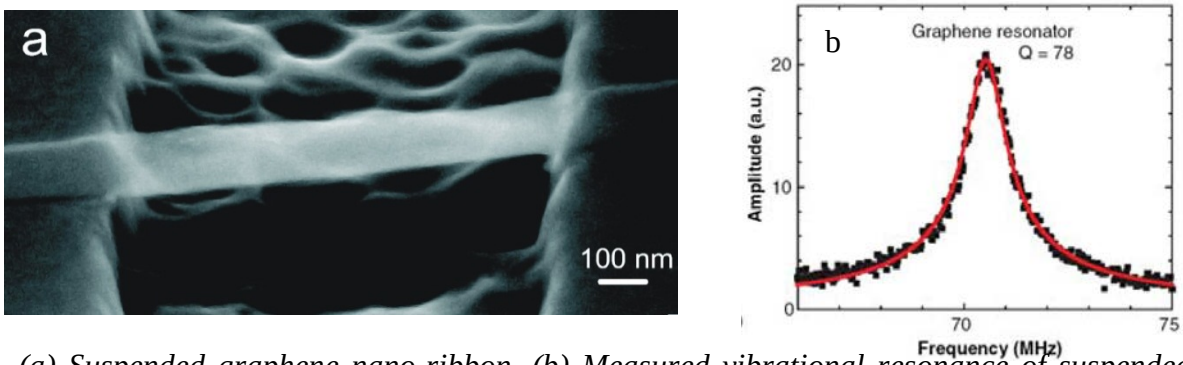

(a) Suspended graphene nano-ribbon. (b) Measured vibrational resonance of suspended graphene sheet.

Suspended graphene holds great promise as material for tunable mechanical resonators. Despite thicknesses all the way down to one atomic layer, the suspended stacks of graphene still maintain high crystalline order, resulting in a NEMS with extraordinarily small thickness, large surface area, low mass density, and high Young's modulus. For instance, a 1μm × 2μm graphene sheet has a mass ~1.5×10^{-18} kg. With a frequency of 100 MHz, it exhibits an effective spring constant k ~ 0.6 N/m. Si_3N_4 resonators of the same size have 100× larger masses with correspondingly smaller frequencies. Because of these excellent material

properties, graphene NEMS hold promise as very good detectors of mass, force and charge, and represent the ultimate limit of two dimensional NEMS.

Regardless of application, a crucial resonator parameter is the quality factor *Q*, determining the width of the resonance. At the outset of the project, the highest demonstrated *Q*s were less than 100 at room temperature. In silicon structures of mm-sized dimensions, *Q*-values in excess of 10^8 have been realized at low temperatures. For future technological applications enhancing Q-factors is thus of great importance and one objective of the project was to demonstrate Q-factors of up to a few thousands are achievable in vacuum.

Since the electronic behaviour of graphene is heavily affected by the presence of a substrate, the suspended graphene structures constitute ideal platforms for analysing intrinsic material properties. These crucially depend on fabrication methods. While the cleanest samples are obtained through mechanical exfoliation, this process is unsuitable for large scale manufacturing. The RODIN project pursued also other methods with the ultimate goal of adapting alternative methods to large scale manufacturing of single layer graphene (SLG). In addition, the RODIN project also strived to investigate the prospects of large scale manufacturing of annealed sp^2-rich diamond-like carbon (DLC) films and few layer poly-crystalline graphene films (FLG) and assess their usefulness for mechanical resonators.

The nano-mechanical resonators hold promise as RF-components which can be used for instance in the front ends of RF-transceivers. There is currently no other technology available that could bring tunability to a high-quality resonator and thus a filter, enabling the adaptivity benefiting current cellular multiradio systems and future cognitive radio architectures.

Using the resonators developed in this project, the RODIN project aimed to investigate possibilities to perform *radio spectrum sensing* using mechanical graphene devices. This includes investigations of the sensitivity and speed of measurement schemes together with a comparison to the more traditional reflection measurement scheme. In the reflection scheme, several resonators can be connected to a single read-out LC-circuit as their frequency-domain signals are fully separable at high Q. By tuning the resonant frequency by tension, substantial regions of radio spectrum can be scanned by a few resonators.

If nanomechanical resonators can be used as tuneable RF-filters, the economic payback is expected to be vast. This is because multiradio front-ends, i.e. band-selection filters, switches, antennas etc, are rapidly becoming a major obstacle in cost- and size-efficient production of mobile phones. The different radio band variants for the second-generation (GSM) and third-generation (WCDMA) cellular standards only are approaching 20, and the trend is increasing along the introduction of the fourth generation (LTE) and the inclusion of complementary radio such as wireless LAN, Bluetooth, satellite navigation (GPS), digital television (DVB-H) etc. Current band-specific radio front-end filters are bulky and expensive, and they cannot be adjusted for reuse in other bands. This problem will be amplified in the future cognitive radio implementation, since no technology exists that could bring the necessary tunability for frequency-agile filtering for e.g. spectrum sensing.

In addition to external RF front-end filters, the circuits within the transceiver itself contain resonators. The present-day commercial radio front-ends are manufactured with CMOS technology, and unfortunately there is no method to manufacture high quality factor tunable resonators with it. This shortcoming restricts the feasible circuit structures, and limits the available performance. Future use of tunable high-Q graphene resonators in conjunction with high integration level CMOS RF IC would allow significant performance improvement. In practice, 3-D integration with flip-chip bonding is a method to couple CMOS IC and graphene die. The sub-circuits of a radio front-end, such as low-noise amplifier (LNA), voltage-controlled oscillator (VCO) and power amplifier (PA), include resonators, and improvement on quality factor and tunability directly leads to improved performance. Higher selectivity, lower noise, and lower power consumption will appear. Present-day trend to use sub-optimal radio architectures, so-called direct conversion receivers, is fundamentally motivated by the fact that no good resonators are available in CMOS. Therefore, graphene – CMOS co-design would, in long term, even change the paradigm of present-day radio electronics, and thus lead to future innovations and increased research activity.

On the longer term it should be recognized that coupling mechanical resonators can also find application in computing. This includes pattern recognition, where complex oscillatory patterns can be stored and retrieved. Developing computing mechanical circuits using graphene is attractive because of small size, high speed, and low power consumption.

An important outcome of the project is the knowledge and technology advancement in the field of nanomanipulation of suspended graphene. To avoid the impact of the substrate on graphene properties, suspended structures may have to be used. This is true also for other devices than nanoresonators. For successful implementation and large scale production of IT-devices or graphene based integrated circuits, the ability to fabricate multiple devices by sculpting a single sheet and applying in-situ post-processing techniques to enhance mobility will be extremely valuable if high yield methods can be realized.

Nanoelectromechanical resonator systems also hold wider potential than just RF-components, for instance in highly sensitive mass sensors and other sensing applications (gas, liquid, protein, lab on chip etc.). For mass sensing, graphene resonators benefit from large target area in combination low mass and high resonant frequencies.

It is likely that the first commercial applications of graphene will not be electronic, but rather mechanical or electromechanical, i.e. “low-tech” products and/or materials benefitting from the strength and/or low mass of graphene and not relying on the details of electron transport that is affected by, e.g., the microscopic structure of graphene edges. The introduction of such products on the market may serve to considerably lower the threshold for the more disruptive graphene based information technology. Thus, easy local access to state-of-the art knowledge and competence regarding the intrinsic mechanical properties and handling of SLG and FLG will be with a competitive edge for emerging start-ups working with graphene composite materials.

Other important application areas include transparent and flexible interconnects and foldable touch displays. In these applications, FLG or annealed DLC-films produced may have advantages compared to SLG. Such electrodes will be more robust, require less tolerance in fabrication, and be more resilient to damage. Because the amount of flexibility that can be tolerated in a graphene based interactive device depends on the amount of deformation (stretching and bending) that can be achieved without significant loss of electrical functionality, hence the RODIN project also aimed at understanding the electromechanical response of few layer graphene and annealed DLC films are relevant for the impact of such applications.

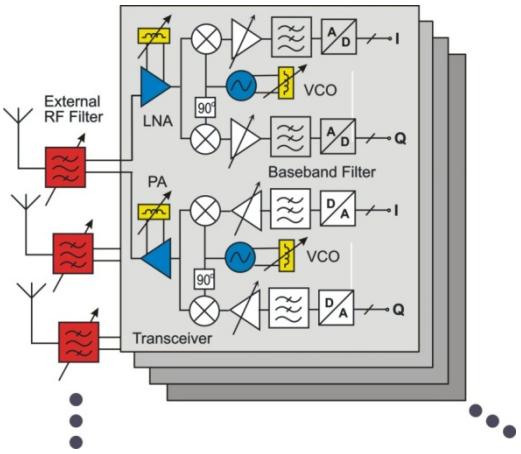

Multi-radio front-end. Components in yellow and red are potential places for a tuneable high-Q resonator.

S&T Results/Foreground

Overall, the results of the RODIN project has been disseminated in 55 peer-reviewed publications and presented over times 75 at international conferences. This section therefore primarily details the development of the demonstrated graphene resonator design for filter applications. While a comprehensive coverage of all scientific results obtained is too long for inclusion in this report, a few highlights relating to objectives other than filter applications are also included.

Demonstration of a graphene resonator

During the initial stages of the RODIN project different designs, fabrication methods and readout schemes were developed. In M24, an assessment of tried and proposed alternatives was made and a decision for a final design was taken.

The RODIN consortium decided to settle for a design of resonators based on wide rectangular multilayer graphene sheets. For the electrical readout method, the direct capacitive transmission scheme was selected. Chips with support electrodes conforming to the above specifications were manufactured in quantity and multilayer graphene sheets were transferred onto the electrodes using different methods. The finished devices were measured electrically and the characteristics together with modelling formed the basis for a CAD-implementation allowing for a filter specification predictions.

To establish the final design parameters the system was first modelled. A capacitively transduced resonator can be modelled with an electrical equivalent circuit consisting of a resistor, a capacitor and an inductor in series, along with a parallel capacitance representing the regular current path.

$$R_{\mathrm{m}} = \frac{\sqrt{km}}{Q\eta^2}, C_{\mathrm{m}} = \frac{\eta^2}{k}, L_{\mathrm{m}} = \frac{m}{\eta^2}$$

$$\eta = V_{\mathrm{dc}} \frac{\partial C}{\partial z} \cong V_{\mathrm{dc}} \frac{\varepsilon WL}{d^2}$$

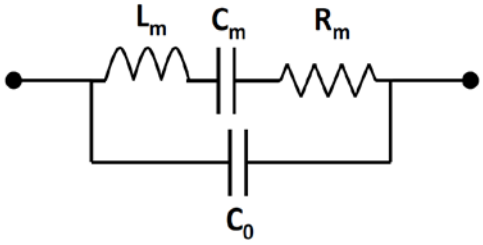

Electronic equivalent circuit for the resonator. C_0 is the electrical capacitance, whereas L_m, C_m and R_m are the motional inductance, capacitance and resistance, respectively. The motional RLC parameters are defined in terms of the effective spring constant k, the mass of the resonator m, and the quality factor Q. The effective electromechanical transduction factor η determines the efficiency of the transduction and depends on the geometrical parameters W, L and d which are the width, length and plate gap of the resonator respectively.

In order to maximize the signal at resonance, the mechanical impedance Z_{m} has to be minimized and, therefore, the transduction factor η must be maximized. As the resonator length L is largely dictated by the resonant frequency, optimal signals can be achieved with wide, narrow-gap devices at high bias. Moreover, based on the definitions of the motional

parameters, a large *Q*-factor, small mass and small spring constant will be beneficial as well.

If the electric field strength of a capacitive graphene resonator is increased on and on (i.e. high V_{dc} and small *d*), the center of the sheet will eventually collapse to the drain electrode at a critical pull-in point. This collapse can be averted, or at least shifted to higher voltages, by using a thicker and stiffer sheet of few-layer graphene. Unfortunately, a stiffer resonator also means that the ability to tune the resonant frequency by adjusting the dc bias will be diminished. Hence, there is a tradeoff between transduction factor on the one hand and tunability on the other.

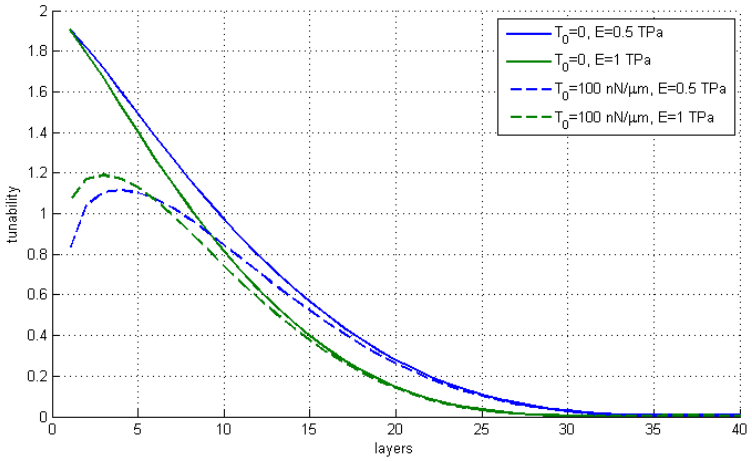

Predicted tunability $(f_{max}-f_{min})/f_{middle}$ *of a few-layer graphene resonator as a function of the number of layers, with L=500 nm, d=100 nm and* V_{dc}*=0–50 V.* T_0 *is the built-in tension and E the Young's modulus, which is ~1 TPa for monolayer graphene and slightly less for few-layer graphene.*

Based on the modelling, in order to maintain some tunability for the resonant frequency, the thickness should be limited to below ~25 layers. For a high-quality graphite sheet of 25 layers, it should be possible to reach a resonant frequency of 1 GHz before a collapse occurs, assuming that there is no electrical breakdown over the narrow electrode gap. Tunability from 0 to 200 V is also very impressive, almost 500 MHz.

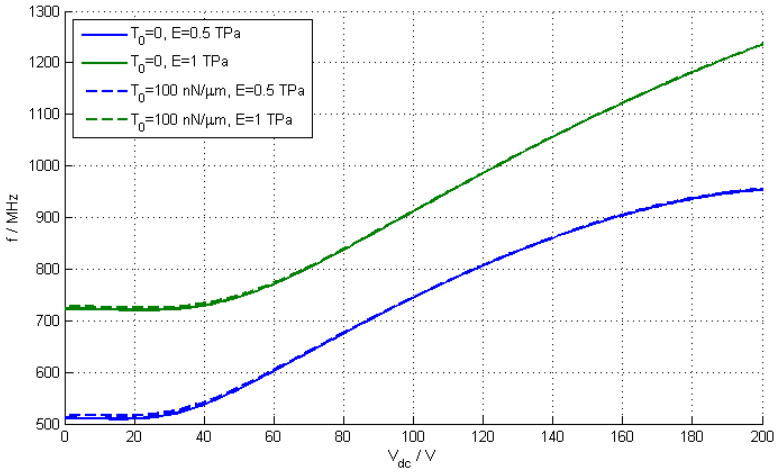

Resonant frequency of a 25-layer graphene sheet as a function of dc bias voltage, with L=500 nm and d=100 nm.

Selecting the parameters from above, namely a 25-layer

resonator with a length L=500 nm and a gap d=100 nm, the impedance at around 1 GHz was calculated from the electrical equivalent circuit. Assuming a device width W=100 µm, a quality factor Q=5000 and a capacitance C_0=0.1 pF, the transmission loss with a 200 V dc bias is only -1 dB at resonance (motional impedance ~12 Ω). Far away from the resonance, the transmission magnitude is determined only by the capacitance C_0 (-25 dB for C_0=0.1 pF).

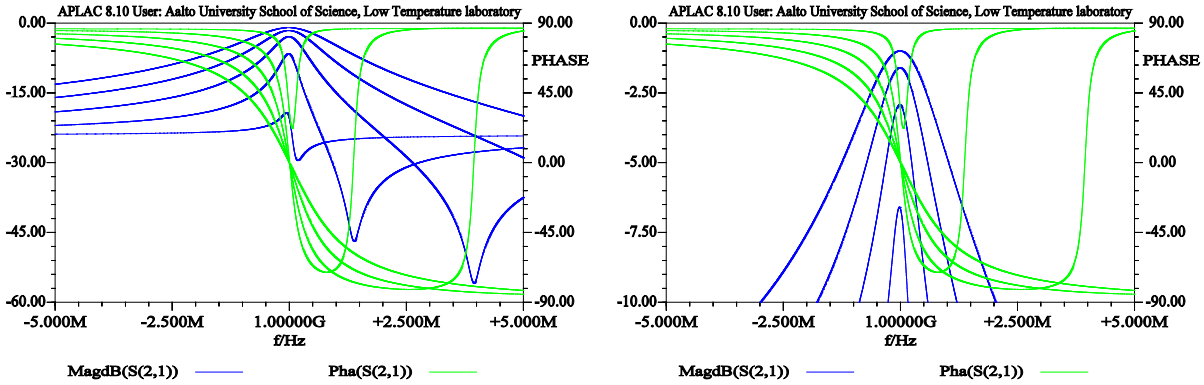

Magnitude and phase of the transmission coefficient S_{21} between 995 and 1005 MHz for the RODIN few-layer resonator design.

To facilitate fabrication of capacitively transduced ultra-wide few layer graphene resonators, two-terminal structures were fabricated starting from an optical lithography process, where the large support electrodes were defined. A 100 mm oxidized high-purity Si wafer was divided into 5-by-5 mm chips, each containing 16 support electrodes as well as one open structure and one short structure for calibration purposes. These support electrodes have a 1-µm-wide and 50-µm-long trench, on top of which the multilayer film was later deposited. After lithography, the large electrodes were deposited using high-vacuum electron-beam evaporation of a Cu/Au or Cu/AuPd bilayer with a typical thickness of 200–400 nm.

In a second step, the wafer was diced using a diamond-bladed saw, and a thin gate electrode was deposited in the middle of each trench using electron-beam lithography (EBL) and thermal evaporation of Cu/Au. These electrodes were typically 400–500 nm wide and about 60 nm thick. Later in the project, support structure chips were fabricated using EBL only, to achieve the best possible precision and to allow for faster testing of different implementations and dimensions.

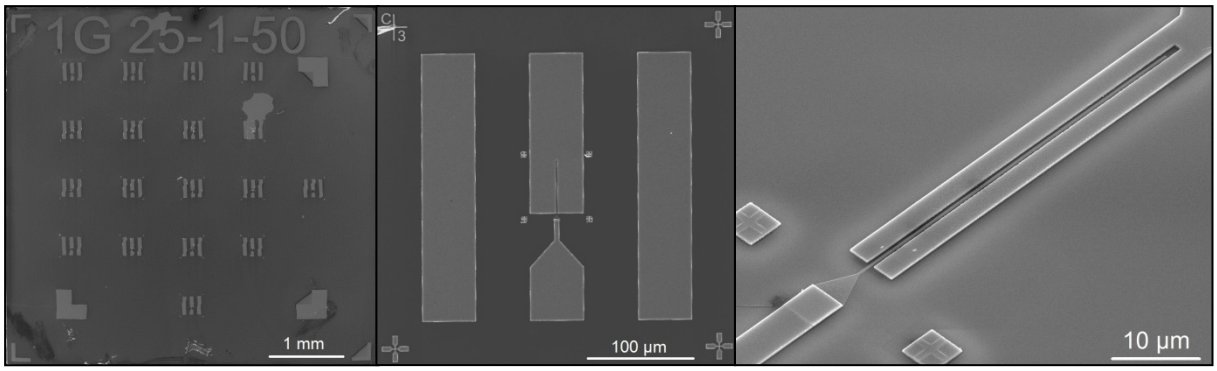

Scanning electron micrographs of RODIN resonator chips before graphene transfer. (left) 5×5 mm chip with 16 normal structures, one open structure and one short structure. (center) Structure with ground electrodes in the ground-signal-ground configuration. (right) Close-up of a support electrode and the thinner gate electrode. The trench is 1 µm wide and 50 µm long.

Three different transfer methods for applying graphene to the chips were used: a wet transfer process, an all-dry transfer technique, and a technique for on-chip exfoliation based on needle micromanipulation.

The wet transfer process employed a setup consisting of an optical microscope as well as a micromanipulator. The first step is to spin coat a Si wafer with PVA and PMMA, and then to deposit graphene flakes using the adhesive tape technique. Single-layer graphene sheets are selected with an optical microscope. The polymer resist and the graphene are then removed from the wafer using wet chemistry with water. The polymer resist and the graphene are removed from the water with a metal plate and transferred with the micromanipulator onto another wafer with predefined electrodes and trenches. The metal plate features a hole, so that the graphene can be aligned onto the predefined electrodes. The polymer is removed with acetone and the device dried using a critical-point dryer. Contamination on the surface is removed by annealing the device in Argon.

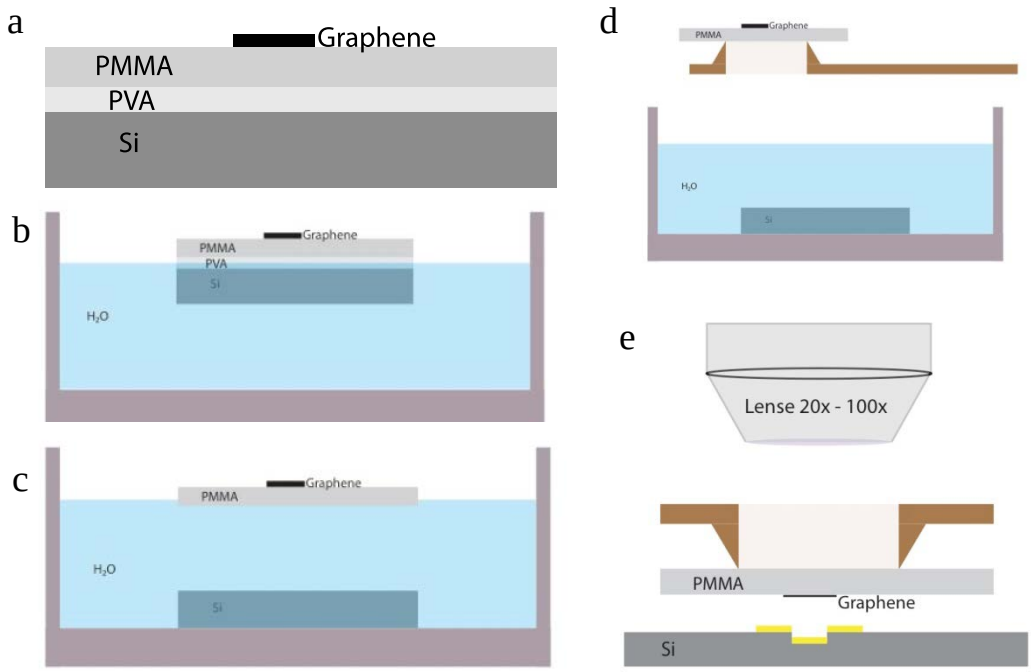

Wet transfer process. (a) Exfoliation of graphene. (b) Wafer placed on water. (c) Dissolution of the PVA layer. (d) Grabbing the PMMA film. (e) Transfer of the PMMA film.

(Left) Optical microscope image of a graphene flake before the transfer. (Right) SEM image of a graphene electromechanical resonator device fabricated with the wet transfer technique. The graphene flake probably contains multiple layers (3-10 layers) since the contrast in the SEM is laraer than for other devices.

The developed all-dry transfer process avoids the contamination appearing in conventional graphene-based NEMS which are fabricated subjecting graphene layers to several steps of nanofabrication, contamination which may alter their electrical and mechanical properties. In the devices fabricated by means of the all-dry-transfer technique the graphene layers are deposited in the very last step of fabrication.

To ensure the cleanness of the graphene layers, the all-dry-transfer technique relies on viscoelastic stamps like the ones used in soft lithography. This process should be contrasted to conventional transfer techniques which involve wet processing of the graphene layers which can contaminate them or introduce ripples and wrinkles during the deposition. We employed commercially available elastomeric films (GelFilm® WF ×4 6.0mil) supplied by Gel-Pak. The Gel-Pak polymer is a polysiloxane based material similar to poly-dimethyl siloxane.

The experimental setup employed to transfer few-layer graphene comprises an optical microscope (Olympus BX 51 supplemented with an Olympus DP25 digital camera) supplemented with large working distance optical objectives, a home-made sample heater and a three axis micrometer stage to accurately position the stamp. The stamp is a thin layer of Gelfilm® which is adhered to a glass slide to facilitate the handling.

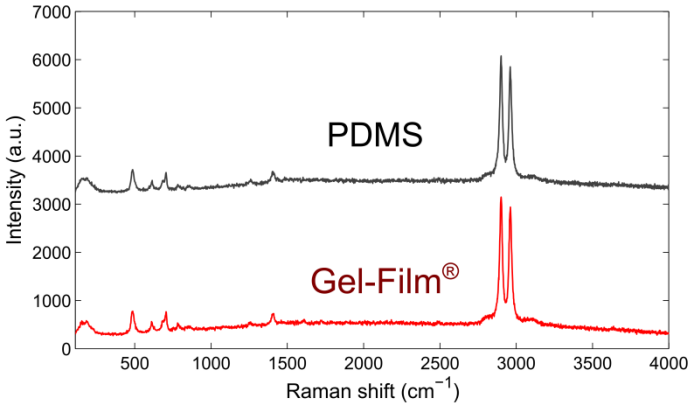

Raman spectra acquired for an in-house fabricated poly-dimethyl siloxane substrate and for a commercially available Gel-Film® substrate.

Few-layer graphene flake are deposited onto the viscoelastic layer by mechanical exfoliation of natural graphite with Nitto tape. The surface of the stamp is inspected under the optical microscope to select the thinner flakes due to their faint contrast under normal and transmission mode illumination. Raman spectroscopy can be carried out on the surface of the stamp to confirm the thickness of the flake. Once a thin flake has been identified, the sample is fixed on the heater with a double side sticky tape and the stamp is attached to the three axis manipulator with the few-layer graphene flakes facing the sample. As the stamp is transparent it allows one to see the sample through it and thus it is possible to align the few-layer graphene flake with some structure on the acceptor surface where one wants to transfer the flake.

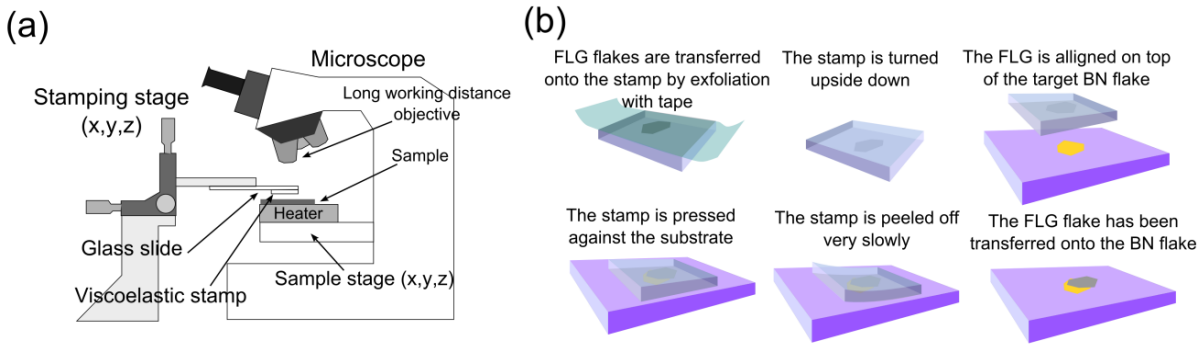

(a) Schematic diagram of the experimental setup employed for the all-dry transfer process. (b) Diagram of the steps involved in the preparation of the viscoelastic stamp and the deterministic transfer of few-layer graphene onto a user-defined location (for instance onto a boron nitride flake).

In order to transfer the few-layer graphene flake to the acceptor surface, the stamp is pressed against the surface and it is peeled off very slowly. The working principle of the transfer is based on the viscoelasticity: the stamp behaves as an elastic solid at short timescales while it can slowly flow at long timescales. Flakes are adhered to its surface because the viscoelastic material flows until getting an intimate contact with the flakes. By slowly peeling off the stamp from the surface, the viscoelastic material flows out releasing the flakes that adhere preferentially to the acceptor surface.

The needle micromanipulation transfer technique was the third method used to directly transfer multilayer graphene flakes onto resonator circuits. In this method, the graphene flakes are initially exfoliated to silicon dioxide substrates, and then a sharp glass needle is used to lift the flakes from the surface. The needle is controlled with a Narishige MMN-1 micromanipulator. The thinnest samples fabricated with this technique were around 35 nm thick, because at smaller thicknesses the glass needle cannot slide under the flake anymore.

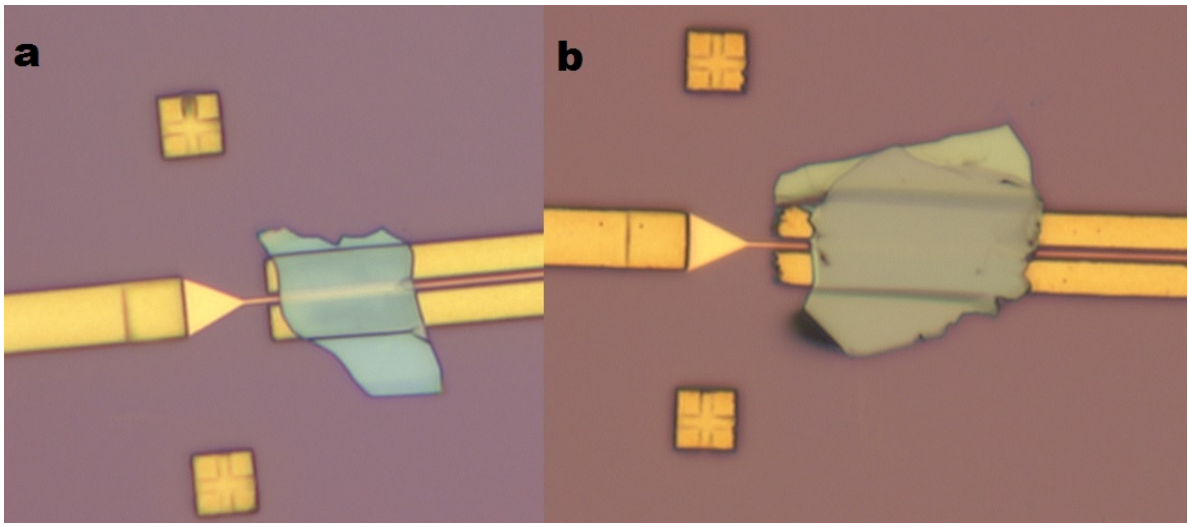

A couple of samples fabricated with needle micromanipulation. The flake in a) is about 35 nm thick, and the flake in b) around 100 nm.

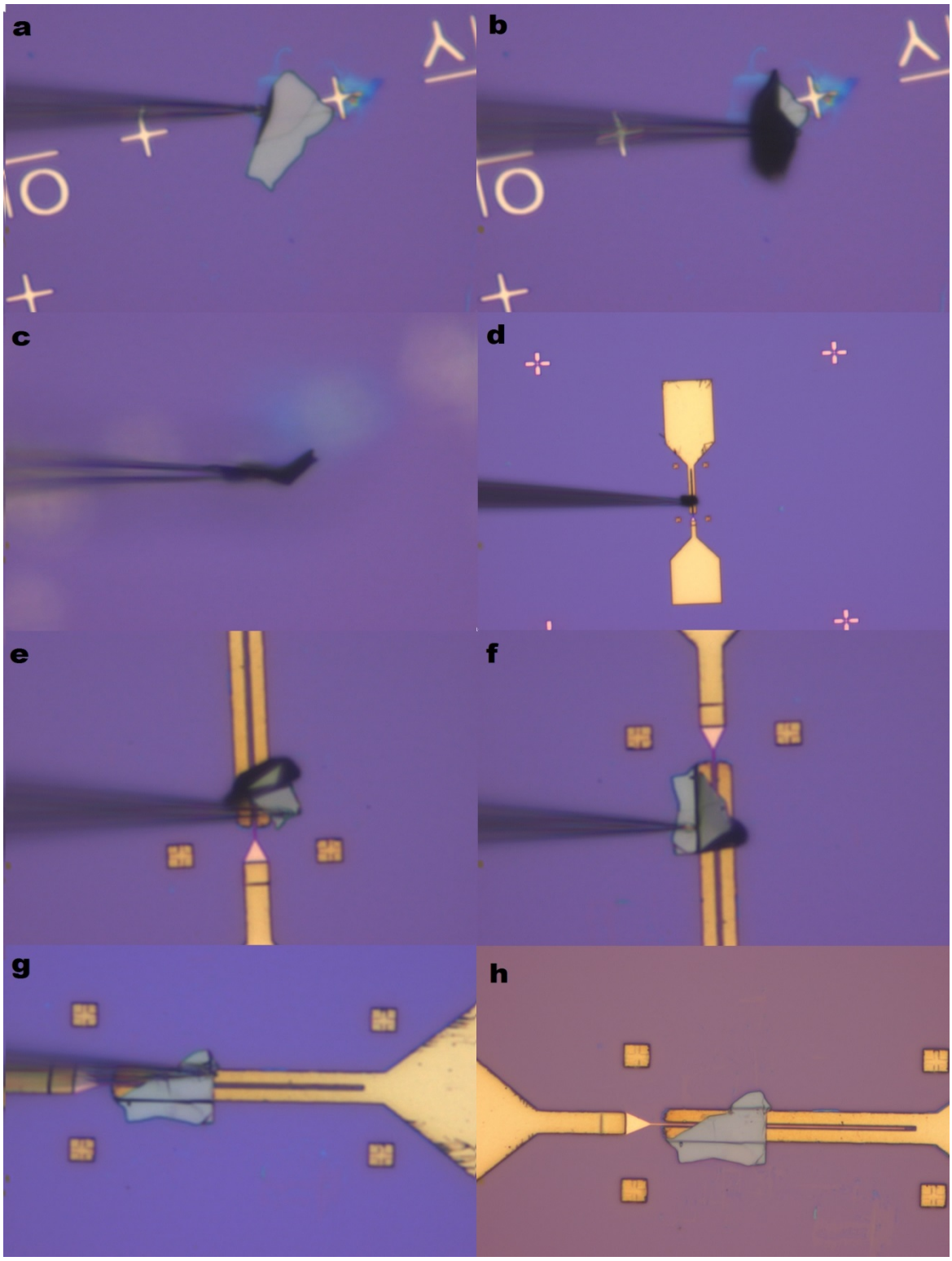

Needle micromanipulation transfer. a) A multilayer graphene flake is exfoliated to an initial SiO_2 substrate. A sharp glass needle tip is positioned under the flake with a micromanipulator. b) – c) The flake is lifted with the tip. d) The flake is positioned onto a resonator circuit. e) The flake adheres poorly to gold, but very well to the SiO_2 surface. f) – g) The flake is first anchored to silicon dioxide, and straightened across the gold electrodes. h) When the flake is smoothened and anchored on both sides, the sample is ready for measurement.

After graphene transfer, the fabricated resonator chips were connected to a measurement circuitry containing an operational amplifier for impedance transformation. The samples were placed inside a vacuum chamber (pressure ~10^{-4} mbar) and the scattering parameters of the devices were measured for several different dc bias voltages using a calibrated vector network analyzer (VNA).

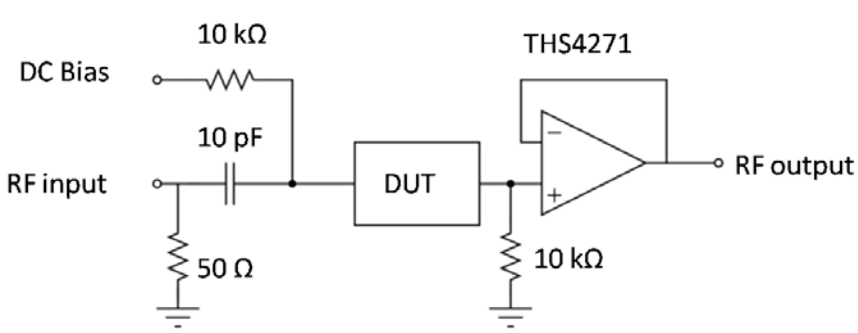

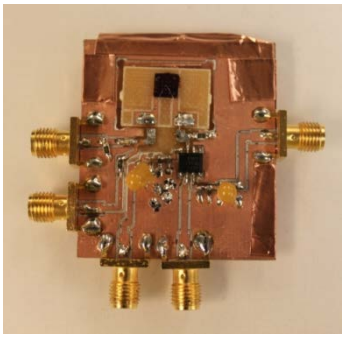

Left: Schematic of the measurement circuitry. An operational amplifier is used for impedance transformation and the dc bias is applied via the 10 kΩ resistors. Right: Measurement PCB with the sample chip at the top.

In total, approximately 20 devices were measured during the project with this technique. Resonances were detected only for one sample, which was of an older single-layer FET-type design. The reason for the poor success in detecting the resonances for the rest of the samples is unclear. It is possible that the vacuum was not good enough, which contributed to breaking of the samples at relatively low bias voltages. At these low dc voltages the resonance magnitude is very small due to the low transduction factor and the relatively large parasitic capacitance, thus making it very difficult to distinguish the weak resonance from the electric noise.

An alternative measurement setup where the RF signal was amplified with two low-noise amplifiers and transmission through the system was measured with a network analyser where then performed. Transmission spectra were recorded as a function of dc bias voltage, which was separated from the RF using bias-tees.

Transmission data was first measured over a large span (~500 MHz), from which the resonance was located and re-measured in more detail. From the transmission data, we determined the resonance frequency as a function of the gate voltage. The result has the characteristic shape of a parabola. Based on the decreasing resonant frequency it is evident that the electrical forces (not tension) are dominant in governing the change of the frequency.

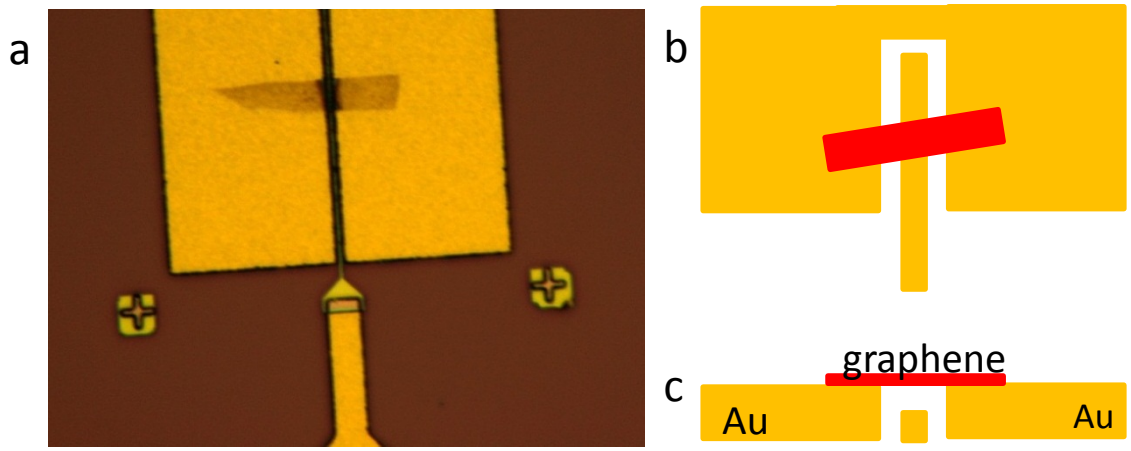

(a) Optical image of a graphene mechanical resonator used to evaluate the performances of graphene as filter. (b,c) Top-view and cross-section of the schematic of the layout.

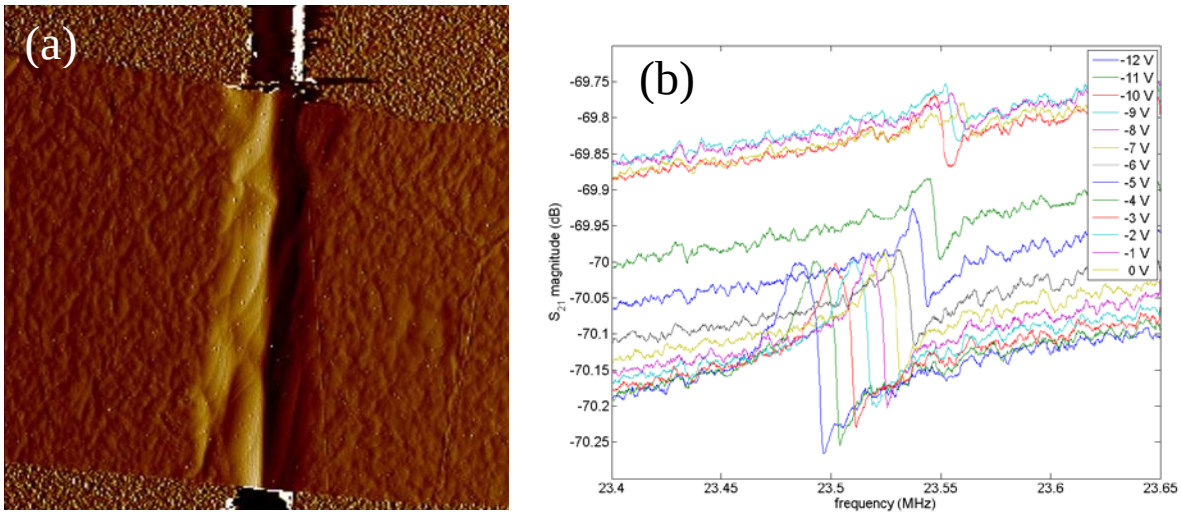

(a) AFM image of a resonator sample. The sample is bulging upwards because of small ridges at the edges of the lithographically patterned gold leads. (b) Transmission through the sample for one of the observed resonances.

We also find that transmission magnitude grows strongly with dc bias. At large dc bias, the peak and the dip in the transmission trace become sharp and their separation can be employed to determine the Q-factor of the mechanical resonator ($Q = f/\Delta f$). The Q-factor was also measured as function of temperature. The measured temperature dependence indicates a typical room temperature quality factor of Q~500.

Based on the comparison between experimental results and theoretical modelling, we assessed the possibilities and limitations of capacitive multilayer graphene resonators in the realization of high-frequency tuneable filters. We have found several factors that contribute to degradation of the performance characteristics of the fabricated multilayer resonators compared to the original theoretical expectations, resulting in a calculated resonator transmission performance that is 40 dB less than originally envisioned.

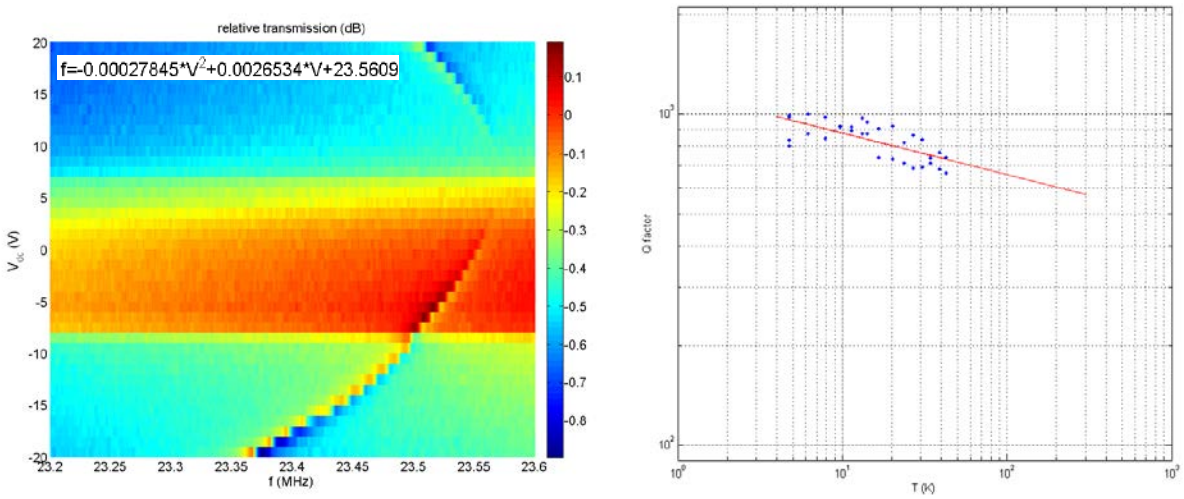

(a) Transmission data of resonator sample. The color scale indicates changes in the transmission magnitude in dB. (b) Q-factor vs. temperature. The solid line indicates power-law type of behavior.

The main degradation factors originate from limited Q-factor of the resonance, strong reduction of the displacement currents due to the mode shape of vibration (factor η), and electrical discharge effects at high dc bias voltages. The expectation in the beginning of the project was that, by increasing tension, one could achieve large Q-factors even at room temperature. Unfortunately, we were limited to values Q < 1000 at T = 300 K. We believe that this is due to the fact that multilayer graphene sticks quite poorly on prefabricated gold electrodes, leading to slippage in the boundary conditions, which prevents efficient tensioning of the material and also leads to additional dissipation via slip at the clamping points.

Originally, we estimated the transduction factor as $\eta = \eta_0 \varepsilon_0 \varepsilon_r V_{\mathrm{dc}} \cdot A/d^2$ with $\eta_0 = 1$, but this turned out to be an untrue assumption. Experiments indicated values in the range of $\eta_0 = 0.1$–0.5, which makes a large difference as the motional impedance values in the electrical equivalent model vary as η^2. In our projected performance analysis, we have employed $\eta_0 = 0.6$, which is an estimate for sinusoidal mode shapes.

The transduction factor is linearly proportional to V_{dc}. In principle, it should be possible to have $V_{\mathrm{dc}} > 100$ V, but often our samples were destroyed at voltages in the range of 50 V. This is especially dependent on irregularities at the edges: a small graphite piece at the edge will be moved by the large electric field leading to discharge and sometimes to shorting of the sample. Consequently, we lose an additional factor of two in the transduction factor because of the reduced dc voltage. The projected characteristics of our resonators when the above limitations are employed in the parameter values were then based on the assumption that the membrane can be tensioned sufficiently to reach the resonant frequency of 1 GHz. Transmission in the pass band becomes -41 dB, which is 40 dB worse than the original goal.

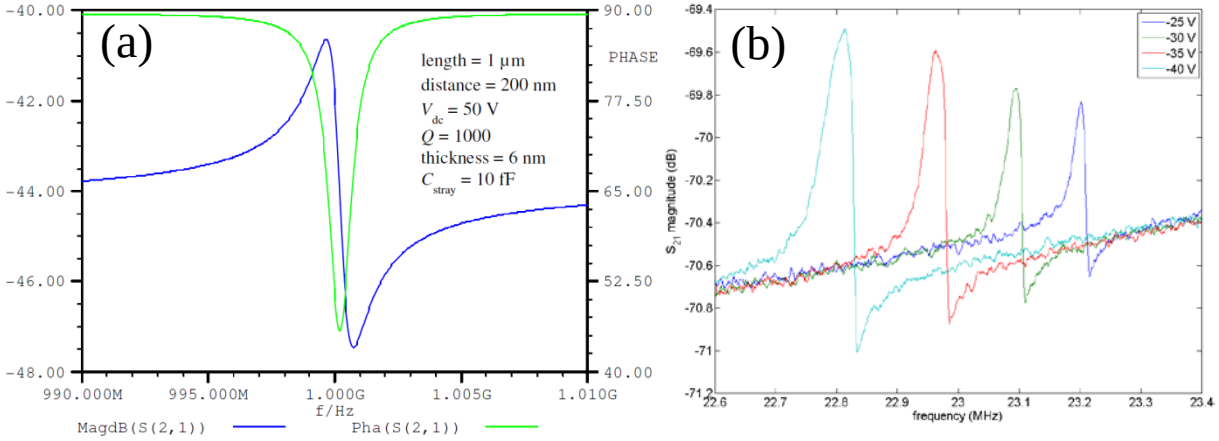

(a) Achievable transmission performance for a 100-micron-wide resonator obtained with the parameter values indicated in the figure and an effective transduction factor of $\eta_0 = 0.6$. *(b) Measured transmission one sample at relatively large dc.*

Based on the performance of the fabricated resonators we then studied and compared various schemes for constructing an optimal filter device out of graphene resonators. In order to achieve a flat passband and steep transition bands a method known as coupled resonator filter synthesis is proposed. It involves using several resonator stages and specific impedance inverters to convert a series resonator into a parallel one. As inductive elements are to be avoided, the impedance inverter will be realized using capacitors only.

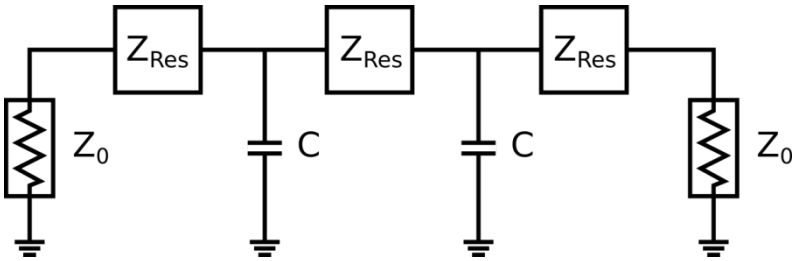

Third-order filter structure used in simulations. Z_{Res} *is the impedance of a graphene resonator.*

A filter consisting of three resonator modules coupled with capacitors was considered. Coupling capacitors were sized as a compromise between bandwidth and passband ripple. Matching the terminal impedances evens the passband ripple out, but this demands high characteristic impedance, up to several kilohms. As an example, to reach the –1 dB target insertion loss, a 10 kOhm terminal impedances is required for a 3-stage filter. Then it is assumed that the actuation of the graphene resonators is ideal, i.e. $\eta_0 = 1$. A lower effective actuation of $\eta_0 = 0.5$ will increase the passband attenuation by ~6 dB. Comparable deterioration of the passband will also be inflicted if the resonator width is decreased or the resonator is made shorter in an attempt to increase the resonance frequency.

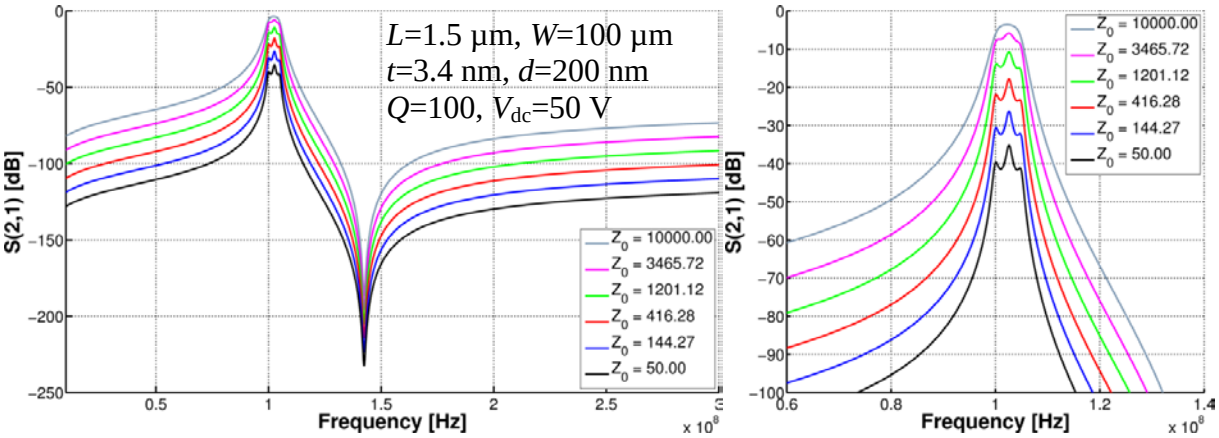

S_{21} parameter of a 3rd-order filter in different source/load impedance environments logarithmically from 50 Ω to 10 kΩ. C=110 fF, W = 100 µm (50 µm for the middle resonator).

These results once again indicate how essential it is to have low characteristic impedance (large η) for the resonators. Depending on the use case, the characteristic impedance of the environment can be higher than the traditional 50 Ω, but even inside an integrated RF circuit it remains below 1 kΩ.

After identifying the reasons for not reaching the original model parameters, the fabricated devices did indeed behave according to modelling. The factors giving rise to the observed performance degradation all can be addressed in a commercial setting. This provided that:

(1) A state-of-the art industrial fab-facility is used to make the chips. This would alleviate the problems with irregularities at the edges which will lead to increased operating voltages, higher frequencies, and better Q-factors.

(2) Better contacting of the FLG to the electrodes. This would significantly reduce the need for large impedance loads and allow the devices to approach the criterion of -1 dB insertion loss in a 50 Ohm environment.

Both problems, (1) and (2), are of a technical nature relating to access to state-of-the art fabrication facilities that were not available to the consortium. The conclusion is that using wide FLG resonators with a capacitive transduction scheme is a feasible route towards tuneable RF-filter components.

Nonlinear damping and record breaking Q-factors

In the RODIN project, the source of dissipation in graphene nanoresonators was investigated both theoretically and experimentally. Reaching a high Q-factor is not only important for RF-filter applications but also for other application areas. Most mechanical resonators damp (slow down) in a well-understood linear manner. In the RODIN project it was discovered that resonators formed from nanoscale graphene and carbon nanotubes exhibit nonlinear damping, opening up exciting possibilities for super-sensitive detectors of force or mass.

In all mechanical resonators studied to date, from large objects several metres in size down to tiny components just a few tens of nanometers in length, damping has always been observed to occur in a highly predictable, linear manner. However, in the RODIN project it was demonstrated that this linear damping paradigm breaks down for resonators with critical dimensions on the atomic scale. Of particular importance we have shown that the damping is strongly nonlinear for resonators based on nanotubes and graphene.

For the graphene resonators exhibiting nonlinear damping, in order to achieve larger quality factors, the driving force was decreased until the motion became barely detectable. For this, it is convenient to select the value of the gate voltage for which the detection signal is largest. In so doing, we measured a quality factor of 100,000 for a graphene resonator at 90 mK. This is the largest quality factor ever reported in a graphene resonator.

The finding has profound consequences. Damping is central to the physics of nanoelectromechanical resonators, lying at the core of quantum and sensing experiments. Therefore many predictions that have been made for nanoscale electro-mechanical devices now need to be revisited when considering nanotube and graphene resonators.

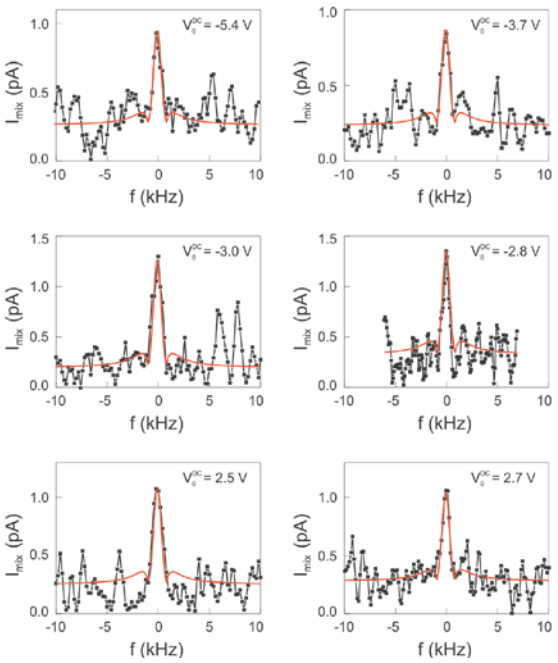

Frequency response of the mixing current for different gate voltages. The red curves are fits with a quality factor of 100,000. Measurements are carried out at 90 mK.

This new insight into the dynamics of nano-scale resonators will also enable dramatic improvements in the performance of numerous devices. Already we have achieved a new record in quality factor for graphene resonators and ultra-weak force sensing with a nanotube resonator.

Measuring bending rigidity of graphene

Although only atomically thick, many of the mechanical properties of graphene membranes can be described by classical continuum mechanics. An important parameter for predicting the performance and linearity of graphene nanoelectromechanical devices as well as for describing ripple formation and other properties such as electron scattering mechanisms, is the bending rigidity, κ. In spite of the importance of this parameter it has so far only been estimated indirectly for monolayer graphene from the phonon spectrum of graphite, estimated from AFM measurements for multilayer graphene (> 8 layers) or predicted from *ab initio* calculations or bond-order potential models. In RODIN we employed a new approach to the experimental determination of κ by exploiting the snap-through instability in pre-buckled graphene membranes. We demonstrated the reproducible fabrication of convex buckled graphene membranes by controlling the thermal stress during the fabrication procedure and showed the abrupt switching from convex to concave geometry that occurs when electrostatic pressure is applied via an underlying gate electrode and how this can be used to extract κ. The value that we obtain for bilayer graphene, $\kappa = 35.5^{+20.0}_{-15.0}$, lies between the two extreme theoretical predictions of $\kappa = 160$ eV (from zero-temperature *ab initio* calculations) and $\kappa = 3$ eV (assuming independent monolayers at room temperature).

In the fabrication of suspended samples (beams and circular/elliptic drums) a controlled compressive strain was built in before under-etching the devices to produce the suspended SLG and FLG. When released, this lead to convex buckled geometries with zero built-in strain. By biasing the back gate, an electrostatic pressure is applied to the membranes. The method used in RODIN is based on relating the snap-through voltage to the local curvature, measured by AFM, and observing at what pressure the membrane undergoes a buckling deformation.

A detailed calculation gives the following expression for the pressure at which the critical deformation is reached

$$p_c = \frac{4\sqrt{\kappa n(\lambda + 2\mu)}}{R_1 R_2}$$

Here R_1 and R_2 are the principal radii of curvature (in orthogonal directions) at the point where the instability starts. As $(\lambda + 2\mu) \approx 340$ Nm^{-1} we can use relation (3) to extract κ from measured values of p_c and $R_{1,2}$.

Results were obtained both for fully clamped circular as well as elliptical membranes. The principal curvatures of the membranes were determined by fitting deflection data from AFM measurements in orthogonal directions. At least six AFM line scans for each membrane where used to fit the radii. The extracted values obtained for the bending rigidity of bilayer membranes was $\kappa = 35.5^{+20.0}_{-15.0}$, eV.

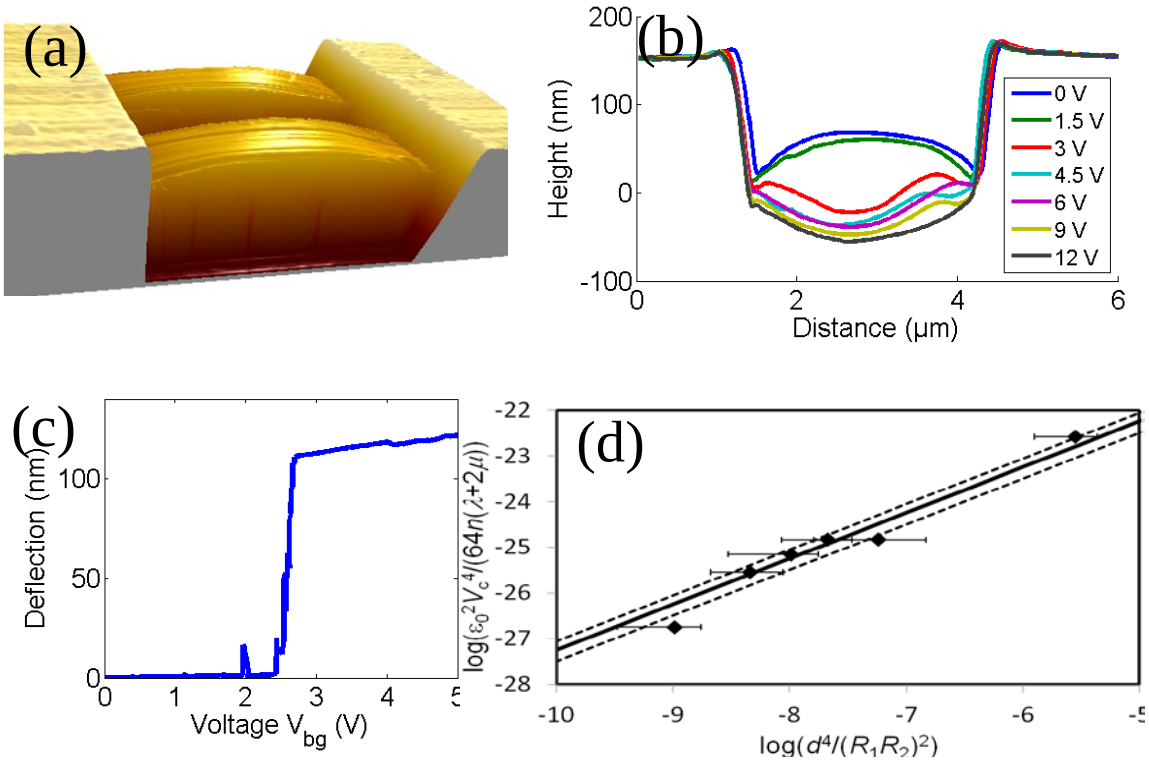

(a) AFM scan of two suspended bilayer beams showing convex buckled shapes. The length of the beams is 2 μm and the centre of the beam is ca. 25 nm higher than the clamped edges. (b) Line scans along the centre of one of the beams as a function of back gate voltage V_{bg}. (c) Deflection versus V_{bg} plot for a same beam measured at the centre of the beam. (d) Plot used to determine κ for fully clamped BLG. κ is determined from the value of the y- intercept at x = 0. Diamonds: average experimental values obtained from fitting the radii of curvature from at least six AFM line scans on each substrate, error bars indicate the standard deviation of the fitted radii. The full line is a straight-line fit to the data and the dashed lines indicate the stated error limits.

Deterministic transfer of shaped-defined graphene flakes

To make graphene devices with well-defined geometries, two steps are required; transfer of the produced graphene and shaping it into the desired geometry. In RODIN a deterministic transfer of shape-defined graphene flakes was developed. Here, micromechanically exfoliated graphene flakes were first shaped and then transferred onto predefined locations on samples with gold electrodes and etched trenches.

The process of shaping the flakes into desired shape was as follows: First, a layer of PMMA was spin-coated onto mechanically exfoliated graphene. Second, frames were e-beam written around pre-selected monolayer flakes. Only a few seconds writing time were required. Development of the PMMA resulted in etching away the frames around the selected flakes. The sample was then exposed to mild oxygen plasma to etch the exposed part of the graphene. Only mild plasma was required for a brief period of time, therefore no defects were

induced in the layers protected by PMMA. The PMMA film was then lifted off using DI water, as in the transfer procedure, while the isolated graphene + PMMA islands remained on the substrate. The PMMA was then dissolved in acetone leaving on the original substrate only the chosen flakes with the shape defined by e- beam lithography. Once shaped and isolated, graphene flakes were transferred using the transfer procedure described above onto the trenches.

As the graphene is invisible during the transfer process, patterns to aid in the alignment were written by e-beam beforehand. After aligning the graphene with the trenches, the samples were left to dry and for some of them the PMMA was dissolved by acetone.

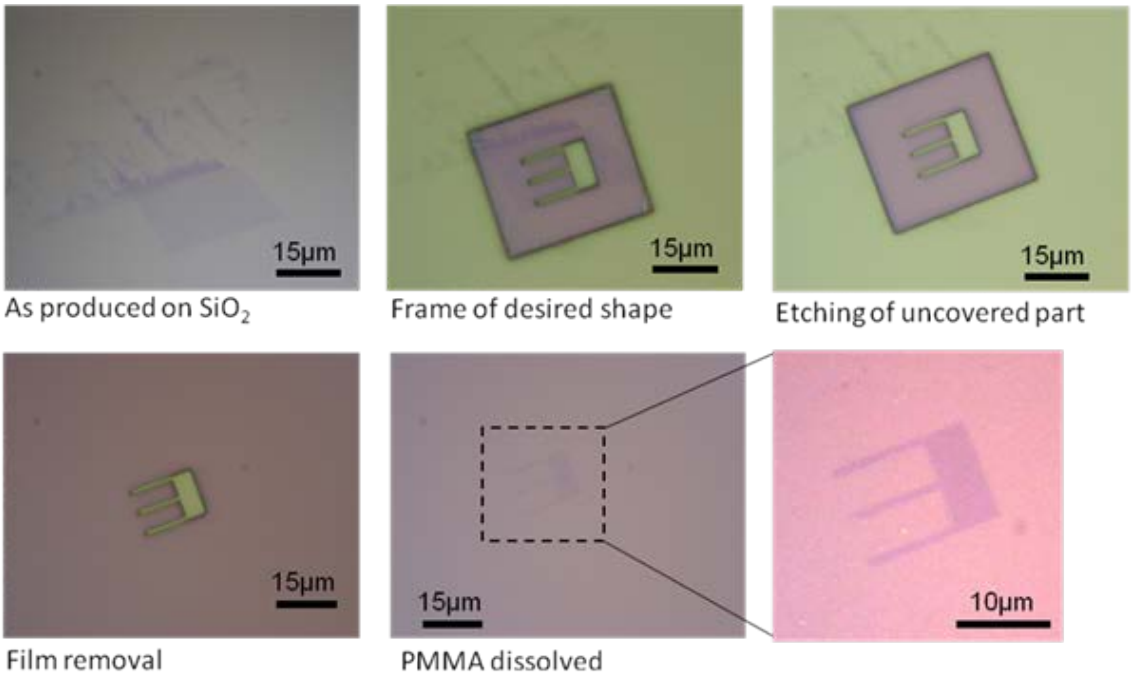

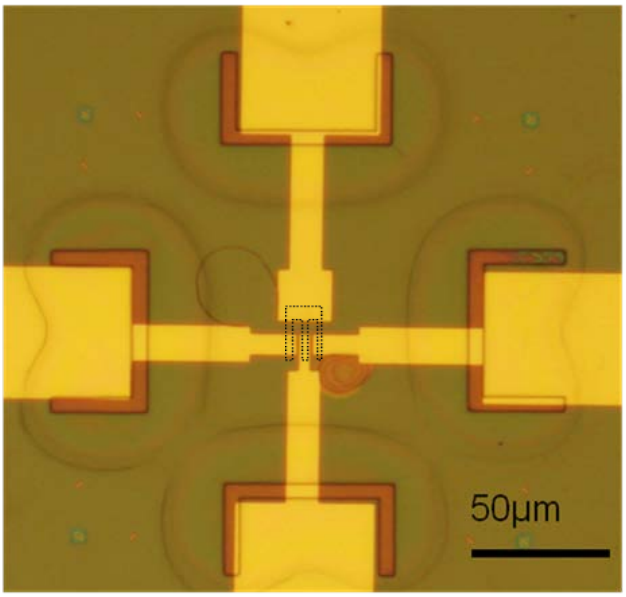

(a) The steps of the inverse transfer process for producing isolated and shape-defined graphene flakes. (b) Graphene shaped following the process of a) was transferred onto electrodes and trenches to form a resonator. The PMMA layer has not yet been dissolved and the alignment patterns to the PMMA via electron beam lithography are visible.

DLC-resonators

In commercial filter applications the attenuation of the pass-band should be reasonably small. In capacitive resonators this can be achieved by increasing the transduction factor, which is proportional to the electric field strength inside the capacitor. Monolayer graphene, although very rigid, will easily strain so much due to electrostatic forces that the capacitor plate snaps to contact. Diamond-like carbon (DLC) averts this problem, as it is stiffer. Moreover, the growth process can be highly customized to adjust the film's thickness, conductivity, compressive stress, Young's modulus and sp^3 content. In the RODIN project we also aimed to compare the performance of DLC-resonators to that of the FLG-resontors.

In our DLC resonator experiments, we used conductive DLC films that had been grown by chemical vapour deposition (CVD) techniques at a temperature of 500 ºC. Typical thickness of the DLC film was around 20 nm, which made the film relatively robust and stiff, but still enabled the resonant frequency to be tuned by several percent. The DLC films were grown on a Si substrate with a 100 nm sacrificial layer of Al or Cu, enabling chemical release of the DLC film from the substrate.

The chips and design used for the DLC-resonators were identical to those of the FLG-resonators. The only difference was that DLC was used instead of FLG as the resonator material.

To deposit DLC onto the chips, the CVD-grown DLC films were first supported from the top by spinning a layer of poly(methyl methacrylate) (PMMA) resist on top of the film. The sacrificial layer was then removed by wet etching in either 10 % HCl (for Al) or $FeCl_3$ (for Cu). The DLC/PMMA membrane was rinsed in DI water and then deposited on the target substrate, directly on top of the support electrode. As a final step, the PMMA layer was removed by baking the chip in a hydrogen atmosphere (5 % H_2 in Ar) at 375 ºC for several hours. Using this procedure, we obtained suspended DLC films with a length of 1 µm, a width up to 50 µm, and a distance to the gate electrode which is typically around 200 nm.

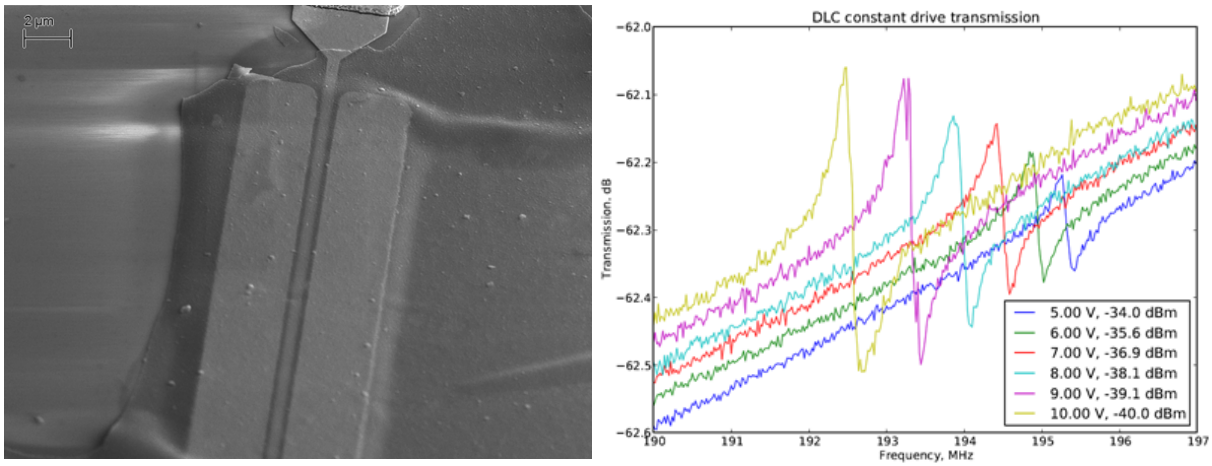

Left: SEM image of a DLC resonator. Right: Transmission through a DLC resonator for different dc voltages at a constant drive. The baseline is given by parasitic and stray capacitances.

Measurements were carried out by applying a dc voltage between the DLC film and the bottom electrode, and resonator motion was actuated by an RF signal. Transmission through the device was measured with a network analyzer as a function of frequency and dc voltage. The resonance frequency of a 1-µm-long, 5-µm-wide and 20-nm-thick DLC membrane was found to be 195.8 MHz at a low dc voltage. By changing the dc voltage up to ±10 V, we observed a frequency tunability of 2 %. The resonance frequency followed a parabolic dependence on the dc voltage, which can be used to estimate that 20 % tunability could be achieved by increasing the voltage up to about 34 V.

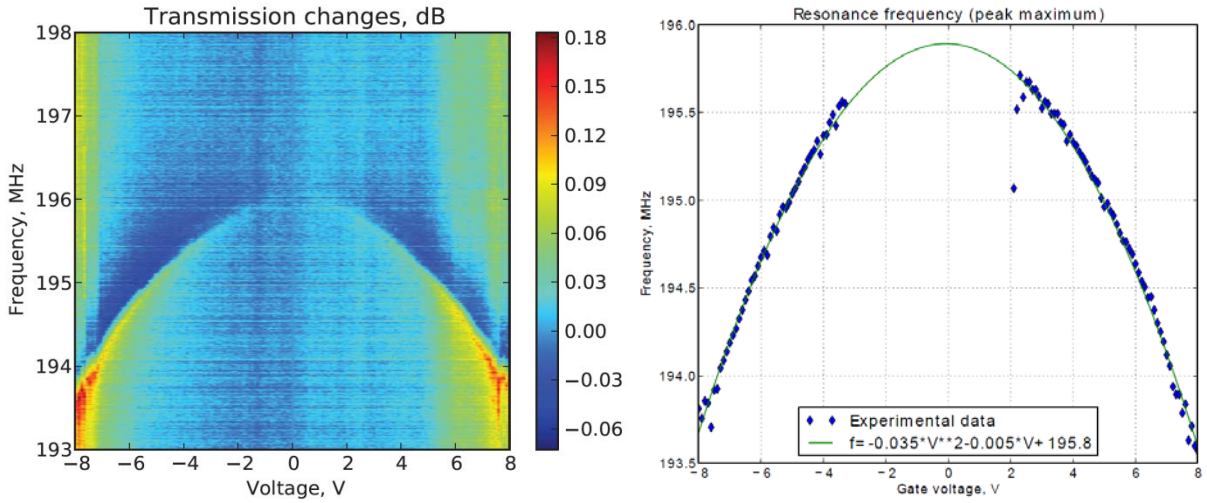

Left: Transmission change as a function of dc voltage and frequency. Right: Resonance frequency (point of maximum transmission) as a function of the dc voltage, including a parabolic fit.

Chemically exfoliated graphene

While micromechanical exfoliation of graphene can be used to produce graphene samples that are of very high quality and also relatively large (~1000s µm^2), the limitation of the process is

that it is labour intensive and the yield of single layer graphene samples is small. Industrial scale production of graphene via this technique is not feasible. Therefore liquid phase exfoliation (LPE) of graphene was studied in the RODIN project as an alternative, scalable graphene production method.

In LPE graphite is exfoliated into individual graphene sheets by chemical wet dispersion followed by ultrasonication, both in aqueous and non-aqueous solvents. Dispersions can be achieved by mild ultrasonication of graphite in water with Sodium Deoxycholate followed by sedimentation based-ultracentrifugation. Bile salt surfactants also allow the isolation of flakes with controlled thickness, when combined with density gradient ultracentrifugation (DGU). In the context of RODIN project, LPE was optimized for the production of printable graphene inks in order to study the deterministic placement of graphene to desired locations via ink-jet printing.

To probe the electrical properties the graphene-ink was printed on Si/SiO_2. To test it as a transparent conductor it was printed on borosilicate glass substrates. The aim was to obtain ink-jet printed drops on substrate, with homogeneous flakes and uniform morphology, i.e. with roughness comparable to the substrate.

The graphene-ink was used to print TFTs with field-effect mobility μ up to ~95$cm^2V^{-1}s^{-1}$. It was also combined with semiconducting polymer PQT-12 to fabricate devices with μ ~0,1 $cm^2V^{-1}s^{-1}$ and ON/OFF ratios of ~4×10^5.

This ink preparation procedure can be generalized to a wide range of layered materials (*e.g.* transition metal dichalcogenides, transition metal oxides, and other two-dimensional compounds such as BN, Bi2Te3, and Bi2Se3) that can also undergo liquid-phase exfoliation.

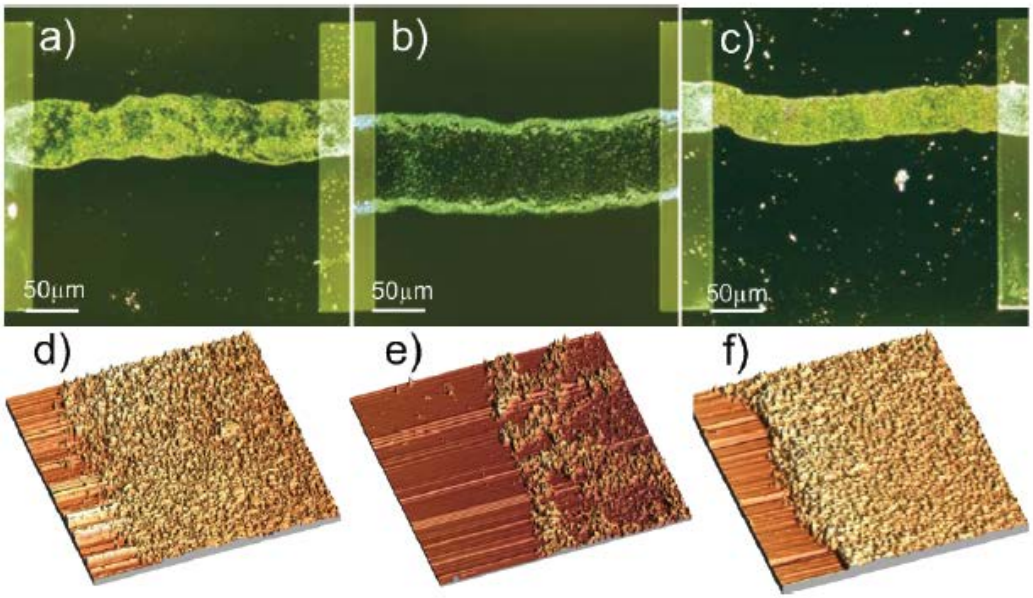

Optical micrographs of ink-jet printed liquid phase exfoliated graphene stripes on a) pristine, b) O_2 and c) HMDS treated substrates. d,e,f) AFM images of a,b,c, respectively.

Potential impact

Important parts of the RODIN project was technology transfer, knowledge transfer between academia and industry, and commercialization. For these reasons, two industrial partners were at the outset included in the RODIN project; One SME, **DIARC**, and one large multinational company, **NOKIA**.

For **DIARC**, which has a strong R&D-component attached to their business model, the main outcome of the project is the direct knowledge transfer relating to materials synthesis, characterization and post-processing from the academic partners. This is necessary in order to ascertain frontline positioning and competitiveness in their business segment.

DIARC will further explore the potential of conductive diamond like carbon as a tunable material for resonators. Other potential new business opportunities for **DIARC** are low impedance metal contacts for graphene materials and few layer graphene fabrication.

While **DIARC** works mainly with amorphous carbon thin film coatings, the industrial partner **NOKIA** was included in order to ensure that technology transfer from academia to industry was carried out concerning use of nanomechanical graphene resonators for RF-filter applications. The main PI at **NOKIA** associated with this task was Dr. Risto Kaunisto. The work by **NOKIA** was intended to cover both work in WP5 relating to assessment for filter applications in radio transceiver front ends as well as work in WP6. The work in WP6 was related to the task T6.2, explicitly stating

"Task T6.2: Dissemination of knowledge, commercialization assessment and technology transfer… produce a baseline costing and assess the potential commercial benefits of the project in industrial partners' markets. Disseminate information to industry. Demonstrate the potential benefits of devices in industrial applications and showcase them to industry. Handling of IPR-issues…"

Already three months into the project, **NOKIA** announced that the division where the PI Dr. Kaunisto worked was sold off to the company **RENESAS**. As Dr. Kaunisto, has expertise in carbon based nanomechanical systems research from previous EU-projects (NANO-RF) and collaboration with academia (NANO-RESO), it was decided to move the person months originally allocated to **NOKIA** to **RENESAS** and include the latter as a partner in the project. The new partner **RENESAS** was not able to commit the same amount of resources to the project as **NOKIA**. It was decided that the work relating to baseline costing and assessing the commercial benefits of the project task T6.2, should be done by the industrial partner, **RENESAS** during the very last phase of the project, i.e. months M35-M36. Work on assessment for filter design in WP5 was mainly transferred to the **AALTO-ECD** node.

However, early in M33, the owners of **RENESAS** announced that the partner **RENESAS**

were to be closed down during a rapid ramp-down during months M33-M35. This effectively prevented Dr. Kaunisto and coworkers to continue to work on the project. The part of task T6.2 concerning baseline costs and assessment of the potential commercial benefits of the design of RODIN FLG nano resonators could thus not be carried out according to plan.

Hence, while results of the research in the project point to the RODIN-resonator design having potential to fulfill the technical specifications required for integration in RF-filters, the commercial potential remain to be evaluated at present. In particular, the possibilities to scale up the developed fabrication methods to industrial quantities must be addressed.

Although the RODIN project has ended, the main partners involved in the development of the resonators (**CHALMERS**, **UCAM-DENG**, **AALTO**, **ICFO**, **TU-DELFT**) are also highly involved in the EU graphene FET-flagship where **NOKIA** is one of the main industrial partners. Hence, close and regular contacts between academia and **NOKIA** will continue within the flagship, presenting further opportunities to carry out the technology transfer and commercialization assessment. **DIARC** also seeks possibilities to continue co-operation with RODIN partners in Flagship and Horizon 2020.

An outcome of the RODIN which deserves mention is the advancement of research on graphene fabrication and manipulation which consolidates the already strong position of European graphene research at the startup phase of the graphene FET-Flagship initiative.

Dissemination

The scientific outcomes of the RODIN project have been presented in 55 scientific peer-reviewed articles and further publications relating to the work in RODIN are planned. The results have also been disseminated by over 75 oral presentations and poster presentations.

While only a handful of the publications are in open-access journals, the vast majority of the publications can be accessed free of charge as they are posted on the Cornell library electronic preprint archive at http://arxiv.org.

Peer-reviewed publications relating to the RODIN project

1. L. Aarik, H. Alles, A. Aidla, T. Kahro, H. Mändar, A. Tamm, R. Rammula, V. Sammelselg, and J. Aarik, Materials Chemistry and Physics (2013). In press.
2. J. Anteroinen, W. Kim, K. Stadius, J. Riikonen, H. Lipsanen and J. Ryynänen, Swedish Radio and Microwave Days, Solna (2012). In press.
3. M. Berdova, S. U. Cho, J.-M. Pirkkalainen, J. Sulkko, X. Song, P. J. Hakonen and M. A. Sillanpää, arXiv:1307.1619 (2013).
4. F. Bonaccorso, A. Lombardo, T. Hasan, Z. Sun, L. Colombo, A. C. Ferrari, Materials Today **15**, 564 (2012).
5. F. Bonaccorso, P.H. Tan, A.C. Ferrari, ACS Nano **7**(3), 1838 (2013).

6. D. Brida, A. Tomadin, C. Manzoni, Y. J. Kim, A. Lombardo, S. Milana, R. R. Nair, K. S. Novoselov, A. C. Ferrari, G. Cerullo, M. Polini, Nature Communications **4**, 1987 (2013).
7. L. G. Cançado, A. Jorio, E. H. Martins Ferreira, F. Stavale, C. A. Achete, R. B. Capaz, M. V. O. Moutinho, A. Lombardo, T. Kulmala, A. C. Ferrari; Nano Lett. **11**,3190 (2011)
8. A. Castellanos-Gomez, M. Poot , G. A. Steele, H. S. J. van der Zant H.S.J., N Agraït, G. Rubio-Bollinger G, Advanced Materials, **24**(6): p. 772-775 (2012).
9. A. Castellanos-Gomez, M. Poot, A. Amor-Amoros, G. A. Steele, H. S. J. van der Zant, N. Agraït, G. Rubio-Bollinger. Submitted (February 2012)
10. A. Castellanos-Gomez, M. Barkelid, A. M. Goossens, V. E. Calado, H. S. J. van der Zant, G. A. Steele. Submitted (March 2012).
11. J. Chaste, A. Eichler, J. Moser, G. Ceballos, R. Rurali, A. Bachtold, Nature Nanotechnology **7**, 301 (2012)
12. J. Chaste, M. Sledzinska, M. Zdrojek, J. Moser, A. Bachtold, Appl. Phys. Lett. **99**, 213502 (2011).
13. K. L. Chiu, M. R. Connolly, A. Cresti, C. Chua, S. J. Chorley, F. Sfigakis, S. Milana, A. C. Ferrari, J. P. Griffiths, G. A. C. Jones, C. G. Smith, Phys. Rev. B **85**, 205452 (2012).
14. M. R. Connolly, K. L. Chiu, A. Lombardo, A. Fasoli, A. C. Ferrari, D. Anderson, G. A. C. Jones, C. G. Smith, Phys. Rev. B. **83**, 115441 (2011).
15. A. Croy, D. Midtvedt, A. Isacsson, J. M. Kinaret, Phys. Rev. B. **86**, 235435 (2012).
16. T. J. Echtermeyer, L. Britnell, S. Milana, A. Lombardo, R. V. Gorbachev, A. N. Grigorenko, A. K. Geim, K. S. Novoselov, A. C. Ferrari, AAPP **89**, 1, C1V89S1P030 (2011).
17. T. J. Echtermeyer, L. Britnell, P. K. Jasnos, A. Lombardo, R. V. Gorbachev,A. N. Grigorenko, A. K. Geim, A. C. Ferrari, K. S. Novoselov, Nature Communications **2**, 458 (2011).
18. A. Eichler, J. Chaste, J. Moser, A. Bachtold , Nano Letters **11**, 2699 (2011).
19. A. Eichler, J. Moser, J. Chaste, M. Zdrojek, I. Wilson-Rae, A. Bachtold, Nature Nanotechnology **6**, 339 (2011).
20. A. Eichler, M. del Álamo Ruiz, J. A. Plaza, A. Bachtold, Phys. Rev. Lett. **109**, 025503 (2012).
21. M. Engel, M. Steiner, A. Lombardo, A. C. Ferrari, H. V. Löhneysen, P. Avouris, R. Krupke, Nature Communications **3**, 906 (2012).
22. A. M. Eriksson, D. M. Midtvedt, A. Croy, and A. Isacsson, Nanotechnology **24**, 395702 (2013).
23. A. C. Ferrari, D. M. Basko, Nature Nanotechnology **8**, 235 (2013).
24. O. Frank, G. Tsoukleri, I. Riaz, K. Papagelis, J. Parthenios, A. C. Ferrari, A. K. Geim, K. S. Novoselov, C. Galiotis, Nature Communications **2**, 255 (2011).
25. Y. Kim,Y. Ma, A. Imambekov, N. G. Kalugin, A. Lombardo, A. C. Ferrari, J. Kono, D. Smirnov, Phys. Rev. B **85**, 121403(R) (2012).
26. Y. Kim, J. M. Poumirol, A. Lombardo, N. G. Kalugin, T. Georgiou, Y. J. Kim, K. S. Novoselov, A. C. Ferrari, J. Kono, O. Kashuba, V. I. Fal'ko, D. Smirnov, Phys. Rev. Lett. **110**, 227402 (2013).
27. P. Klar, E. Lidorikis, A. Eckmann, I. A. Verzhbitskiy, A. C. Ferrari, C. Casiraghi, Phys. Rev. B **87**, 205435 (2013).

28. A. A. Lagatsky, Z. Sun, T. S. Kulmala, R. S. Sundaram, S. Milana, F. Torrisi, O. L. Antipov, Y. Lee, J. H. Ahn, C. T. A. Brown, W. Sibbett, A.C. Ferrari, Appl. Phys. Lett. **102**, 013113 (2013).
29. N. Lindahl, D. Midtvedt, J. Svensson, O. A. Nerushev, N. Lindvall, A. Isacsson, E. E. B. Campbell, Nano Letters **12**(7), 3526 (2012).
30. Y. Ma, Y. Kim, N. G. Kalugin, A. Lombardo, A. C. Ferrari, J. Kono, A. Imambekov, D. Smirnov, arXiv:1304.5415 (2013).
31. O. M. Maragò, P. H. Jones, P. G. Gucciardi, G. Volpe, A. C. Ferrari ; Nature Nanotechnology **8**, 807 (2013).
32. J. Mertens, A. L. Eiden, D. O. Sigle, A. Lombardo, Z. Sun, R. S. Sundaram, A. Colli, C. Tserkezis, J. Aizpurua, S. Milana, A. C. Ferrari, J. J. Baumberg; Nano Lett., doi: 10.1021/nl4018463 (2013).
33. D. Midtvedt, Z. Qi, A. Croy, H. Park, and A. Isacsson, arXiv:1309.1622 (2013).
34. J. Moser, J. Güttinger, A. Eichler, M. J. Esplandiu, D. E. Liu, M. I. Dykman, A. Bachtold, Nature Nanotechnology **8**, 493 (2013).
35. A. Nathan, A. Ahnood, M. T. Cole, S. Lee, Y. Suzuki, P. Hiralal, F. Bonaccorso, T. Hasan, L. Garcia-Gancedo, A. Dyadyusha, S. Haque, P. Andrew, S. Hofmann, J. Moultrie, D. Chu, A. J. Flewitt, A. C. Ferrari, M. J. Kelly, J. Robertson, G. A. J. Amaratunga, W. I. Milne; P IEEE 100, 1486 (2012).
36. M. Oksanen, A. Uppstu, A. Laitinen, D. J. Cox, M. Craciun, S. Russo, A. Harju and P. Hakonen, arXiv:1306.1212 (2013).
37. P. Pasanen, M. Voutilainen, M. Helle, X. Song and P. J. Hakonen, Phys. Scr. **T146**, 014025 (2012).
38. M. Poot and H.S.J. van der Zant, Phys. Reports **511**, 273-336 (2012).
39. D. Popa, Z. Sun, T. Hasan, F. Torrisi, F. Wang, A. C. Ferrari, Appl. Phys. Lett. **98**, 073106 (2011).
40. R. K. Puddy, P. H. Scard, D. Tyndall, M. R. Connolly, C. G. Smith, G. A. C. Jones, A. Lombardo, A. C. Ferrari, M. R. Buitelaar, Appl. Phys. Lett. **98**, 133120 (2011).
41. R. Rammula, L. Aarik, A. Kasikov, J. Kozlova, T. Kahro, A. Niilisk, L. Matisen, H. Alles, and J. Aarik, IOP Conferenece Series: Materials Science and Engineering (2013).
42. M. A. Sillanpää, R. Khan, R., T. T. Heikkilä, and P. J. Hakonen, Phys. Rev. B **84**, 195433 (2011).
43. X. Song, M. Oksanen, M. A. Sillanpää, H. G. Craighead, J. M. Parpia, and P. J. Hakonen, Nano Letters **12**, p. 198-202 (2012).
44. Z. Sun, T. Hasan, A. C. Ferrari Physica E **44**, 1082 (2012).
45. J. Svensson, N. Lindahl, H. Yun, M. Seo, D. Midtvedt, Y. Tarakanov, N. Lindvall, O. Nerushev, J. M. Kinaret, S.W. Lee, E. E. B. Campbell, Nano Letters **11**, 3569 (2011).
46. P. H. Tan, W. P. Han, W. J. Zhao, Z. H. Wu, K. Chang, H. Wang, Y. F. Wang, N. Bonini, N. Marzari, N. Pugno, G. Savini, A. Lombardo, A. C. Ferrari, Nature Materials **11**, 294 (2012).
47. Z. Tan, A. Puska, T. Nieminen, F. Duerr, C. Gould, L. W. Molenkamp, B. Trauzettel and P. J. Hakonen, arXiv:1308.5947 (2013).
48. C. Thiele, A. Felten, T. J. Echtermeyer, A. C. Ferrari, C. Casiraghi, H. v. Löhneysen, R. Krupke, Carbon **64**, 84 (2013).

49. A. Tomadin, D. Brida, G. Cerullo, A. C. Ferrari, M. Polini; Phys. Rev. B **88**, 035430 (2013).
50. F. Torrisi, T. Hasan, W. Wu, Z. Sun, A. Lombardo, T. Kulmala, G. W. Hshieh, S. J. Jung, F. Bonaccorso, P. J. Paul, D. P. Chu, A. C. Ferrari; ACS Nano **6**, 2992 (2012).
51. I. Tsioutsios, J. Moser, J. A. Plaza, A. Bachtold, J. Appl. Phys. **114**, 104310 (2013).
52. L. Vicarelli, M.S. Vitiello, D. Coquillat, A. Lombardo, A.C. Ferrari, W. Knap, M. Polini, V. Pellegrini, A. Tredicucci; Nature Materials **11**, 865 (2012).
53. J. K. Viljas, A. Fay, M. Wiesner, and P. J. Hakonen, Phys. Rev. B **83** 205421 (2011).
54. J. Voutilainen, A. Fay, P. Häkkinen, J. K. Viljas, T. T. Heikkilä, and P. J. Hakonen, Phys. Rev. B **84**, 045419 (2011).
55. C.A. Zaugg, Z. Sun, V. J. Wittwer, D. Popa, S. Milana, T. Kulmala, R. S. Sundaram, M. Mangold, O. D. Sieber, M. Golling, Y. Lee, J. H. Ahn, A. C. Ferrari, U. Keller ; arxiv:1310.2132 (2013).
56. M. Zhang, E. J. R. Kelleher, F. Torrisi, Z. Sun, T. Hasan, D. Popa, F. Wang, A. C. Ferrari, S. V. Popov, J. R. Taylor; Optics Express **20**, 25077 (2012).
57. W. J. Zhao, P. H. Tan, J. Liu, A. C. Ferrari; J. Am. Chem. Soc. **133**, 5941 (2011).